AIP | Applied Physics Letters

Role of collisional broadening in Monte Carlo simulations of terahertz quantum cascade lasers

Alpar Matyas, Paolo Lugli, and Christian Jirauschek

Citation: Appl. Phys. Lett. **102**, 011101 (2013); doi: 10.1063/1.4773516
View online: http://dx.doi.org/10.1063/1.4773516
View Table of Contents: http://apl.aip.org/resource/1/APPLAB/v102/i1
Published by the American Institute of Physics.

Related Articles

Master-oscillator power-amplifier quantum cascade laser array
Appl. Phys. Lett. 101, 261117 (2012)

Widely tuned room temperature terahertz quantum cascade laser sources based on difference-frequency generation
Appl. Phys. Lett. 101, 251121 (2012)

Noise amplification by chaotic dynamics in a delayed feedback laser system and its application to nondeterministic random bit generation
Chaos 22, 047513 (2012)

Effect of the number of quantum dot layers and dual state emission on the performance of InAs/InGaAs passively mode-locked lasers
Appl. Phys. Lett. 101, 251115 (2012)

Ultrafast polarization modulation in vertical cavity surface emitting lasers with frequency dependent current injection
Appl. Phys. Lett. 101, 251104 (2012)

Additional information on Appl. Phys. Lett.

Journal Homepage: http://apl.aip.org/
Journal Information: http://apl.aip.org/about/about_the_journal
Top downloads: http://apl.aip.org/features/most_downloaded
Information for Authors: http://apl.aip.org/authors

ADVERTISEMENT

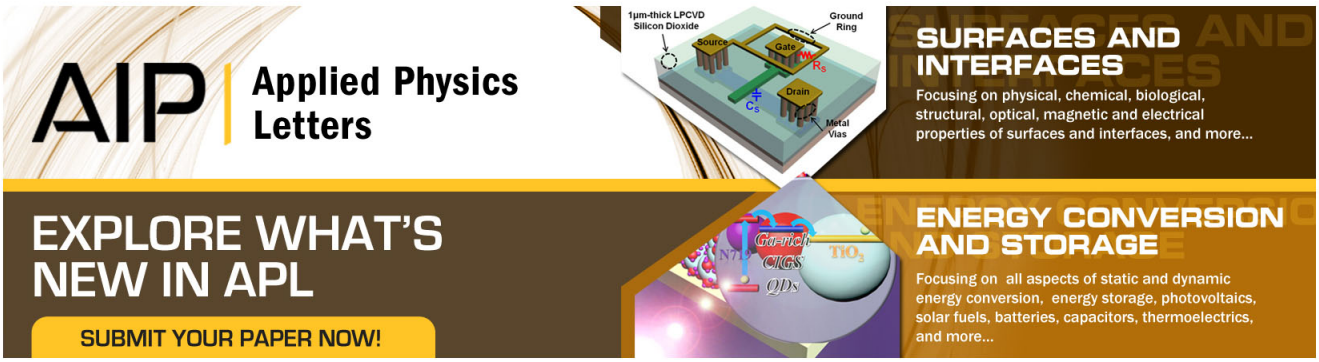

Role of collisional broadening in Monte Carlo simulations of terahertz quantum cascade lasers

Alpar Matyas,[a] Paolo Lugli, and Christian Jirauschek
Institute for Nanoelectronics, Technische Universität München, D-80333 Munich, Germany

(Received 26 September 2012; accepted 13 December 2012; published online 2 January 2013)

Using a generalized version of Fermi's golden rule, collisional broadening is self-consistently implemented into ensemble Monte Carlo carrier transport simulations, and its effect on the transport and optical properties of terahertz quantum cascade lasers is investigated. The inclusion of broadening yields improved agreement with the experiment, without a significant increase of the numerical load. Specifically, this effect is crucial for a correct modeling at low biases. In the lasing regime, broadening can lead to significantly reduced optical gain and output power, affecting the obtained current-voltage characteristics. © *2013 American Institute of Physics*. [http://dx.doi.org/10.1063/1.4773516]

Quantum cascade lasers (QCLs) are among the few coherent sources that can generate terahertz radiation with milliwatt output powers.[1] From a practical point of view, terahertz QCLs are very compact and robust; however, the most challenging goal remains the increase of the maximum operating temperature.[2,3] Detailed modeling by a wide range of simulation tools based on semiclassical and fully quantum mechanical methods has led to an improved understanding of the physical processes in terahertz QCLs. Common approaches include the non-equilibrium Green's functions (NEGF),[4–6] density matrix,[7,8] and semiclassical ensemble Monte Carlo (EMC) methods,[9–13] as well as rate equation-based models.[14,15] While each of these approaches has advantages and drawbacks, all of them use approximations and must be applied carefully. One of the first approaches applied for the modeling of terahertz heterostructures has been the EMC method, which is based on the semiclassical Boltzmann equation and Fermi's golden rule.[9] EMC methods offer a relatively low numerical complexity as compared to quantum transport approaches and a straightforward extraction of physical quantities, and can model the time dependence of physical processes;[16] however, they do not account for the influence of quantum effects on the carrier transport. A complete inclusion of these effects requires a full quantum approach such as NEGF or density matrices, hence losing the relative efficiency and simplicity of semiclassical descriptions. Here, we follow a different approach, implementing certain aspects of the quantum transport theory into EMC, however, preserving the overall structure of the algorithm and its associated advantages. We focus on the discrete level eigenenergies in the absence of broadening mechanisms entering Fermi's golden rule formulation of EMC, and leading, for example, to an underestimation of the simulated currents in the low-bias range (LBR) of QCLs.[17] For bulk semiconductor structures, it has been shown that the linewidth of the energetic states due to collisional broadening (CB) can be taken into account in EMC by replacing the delta function in Fermi's golden rule with a Lorentzian function of finite linewidth.[18,19] In this letter, we develop the Lorentzian broadening for quantum well structures such as QCLs, and include it in our semiclassical EMC method. Furthermore, we investigate the influence of this correction on the simulation results for transport and optical properties of terahertz QCLs.

The scattering processes in semiclassical EMC methods fulfill energy conservation for a single scattering event due to the discrete eigenenergies.[18,19] Here, we relax this constraint and require only the expectation value of the scattering transitions to be energy conserving.[19] We start from the evolution equation for the density matrix elements ρ_{ij} of the form[20]

$$\partial_t \rho_{ij} = -\mathrm{i}\,\omega_{ij}\rho_{ij} + \frac{1}{\mathrm{i}\hbar}\sum_{\ell}(H'_{i\ell}\rho_{\ell j} - \rho_{i\ell}H'_{\ell j}) + \partial_t \rho_{ij}|_{\mathrm{relax}}, \quad (1)$$

where the third term is the relaxation term, introducing decoherence effects for the temporal evolution of the off-diagonal matrix elements. The Hamiltonian H' describes a perturbation in the form of a scattering mechanism, where we, for now, restrict ourselves to time independent processes, such as impurity or interface roughness scattering.[21] Furthermore, $\omega_{ij} = (\epsilon_i - \epsilon_j)/\hbar$, where $\epsilon_i = E_\lambda + \hbar^2\mathbf{k}^2/2m^*$ is the total energy of the electron in state $|i\rangle = |\lambda\mathbf{k}\rangle$, with subband index λ and electron wavevector $\mathbf{k}$. We extend our semiclassical EMC framework based on a generalization of Fermi's golden rule, obtained from Eq. (1). This approach is applied to the evaluation of intersubband processes (i.e., $\lambda_1 \neq \lambda_2$) in our EMC code.

The relaxation term can be written in the general form $\partial_t \rho_{ij}|_{\mathrm{relax}} = \sum_{mn}\Gamma_{ijmn}\rho_{mn}$, where Γ is the scattering superoperator.[21] This term has to be brought into a form compatible with EMC, which delivers semiclassical scattering rates r_{ij} from state $|i\rangle$ to $|j\rangle$.[21] To this end, we have to neglect nondiagonal scattering contributions,[5] and only consider transitions between different subbands for the dephasing,[13] since the intersubband coherence in two-dimensional electron systems is ideally not affected by the intrasubband interactions.[22] In fact, the inclusion of intrasubband scattering events would lead to a serious overestimation of the dephasing in the chosen approach.[4] As a result, the term becomes $\partial_t \rho_{ij}|_{\mathrm{relax}} = -\gamma_{ij}\rho_{ij}$ for the off-diagonal matrix elements, where $\gamma_{ij} = (\gamma_i + \gamma_j)/2$ is the semiclassical dephasing rate;[13,20] here, γ_i is the total out-scattering rate from state $|i\rangle$ to all states in other subbands.[13]

[a]Electronic mail: alparmat@mytum.de. URL: http://www.nano.ei.tum.de.

 © 2013 American Institute of Physics

This corresponds to a lifetime broadening approach, which neglects effects such as pure dephasing contributions.[20] We now solve Eq. (1) for ρ_{ij} with $i \neq j$. In our calculation, we assume that the diagonal matrix elements are dominant, thus neglecting the contribution of the off-diagonal matrix elements besides ρ_{ij}, which is always justified for strong dephasing. Furthermore, we restrict ourselves to the stationary operating regime, where the diagonal matrix elements ρ_{ii} are constant due to a balance of in- and out-scattering events. The steady state solution for ρ_{ij} is then obtained by setting $\partial_t \rho_{ij} = 0$. With $\tilde{\omega}_{ij} = (\epsilon_i - \epsilon_j + H'_{ii} - H'_{jj})/\hbar$, we obtain

$$\rho_{ij} = \frac{1}{\hbar} H'_{ij} \frac{\rho_{jj} - \rho_{ii}}{\mathrm{i}\gamma_{ij} - \tilde{\omega}_{ij}}. \tag{2}$$

For $i=j$, Eq. (1) directly yields the transition rates. For the term containing the sum in Eq. (1), we only consider $\ell = i,j$ to obtain the transition rate from state $|i\rangle$ to a final state $|j\rangle$. Furthermore, inserting Eq. (2) for the off-diagonal matrix elements, we obtain

$$\partial_t \rho_{jj}\big|_{i\to j} = -\partial_t \rho_{ii}\big|_{i\to j} = \frac{2}{\hbar^2} \left|H'_{ij}\right|^2 (\rho_{ii} - \rho_{jj}) \frac{\gamma_{ij}}{\gamma_{ij}^2 + \tilde{\omega}_{ij}^2}. \tag{3}$$

Transitions from state $|j\rangle$ to $|i\rangle$ are treated separately, i.e., back-scattering events from $|j\rangle$ are not included. The single-electron transition rate is obtained by normalization to the electron number in the initial level ρ_{ii}. Thus, we obtain for the scattering mechanism associated with the Hamiltonian H' the rate

$$r'_{i\to j} = \frac{2}{\hbar^2} \left|H'_{ij}\right|^2 \frac{\gamma_{ij}}{\gamma_{ij}^2 + \tilde{\omega}_{ij}^2}. \tag{4}$$

We set $\tilde{\omega}_{ij} \approx \omega_{ij}$ in the following, neglecting the frequency shift due to the diagonal Hamiltonian matrix elements. For $\gamma_{ij} \to 0$, the Lorentzian in Eq. (4) approaches a delta function $\pi\delta(\omega_{ij})$, thus Fermi's golden rule is recovered. For Hamiltonians with harmonic time dependence $\tilde{H}'_{ij}(t) = \Re\{H'_{ij}\exp(-\mathrm{i}\omega t)\}$, describing effects such as scattering with phonons or photons, an expression analogous to Eq. (4) can be derived using the rotating wave approximation.[23] The corresponding rate is

$$r'_{i\to j} = \frac{2}{\hbar^2} \left|H'_{ij}\right|^2 \frac{\gamma_{ij}}{\gamma_{ij}^2 + (\omega_{ij} \pm \omega)^2}, \tag{5}$$

where the $+$ and $-$ denote absorption and emission events, respectively.

In the following, we discuss the implementation of the CB corrections in EMC. Intersubband scattering is now treated based on Eqs. (4) and (5). This means that the energy conserving delta function in Fermi's golden rule is replaced by a Lorentzian, involving some additional computational effort. However, the overall numerical load is not significantly increased as compared to conventional EMC, since the computation of the scattering form factors and the time-dependent simulation algorithm remains unchanged. The final wavevector $\mathbf{k}'$ is now not given by energy conservation like in the conventional EMC, but randomly chosen according to Eqs. (4) and (5), respectively. This means that energy conservation is obtained only for the expectation value of the transition energy.[19] For the numerical evaluation, we cut off the Lorentzian at 10^{-3} of its peak value. Intrasubband transitions are still treated conventionally in our EMC code. Also, intercarrier scattering is evaluated based on Fermi's golden rule due to its significantly increased complexity and computational load as compared to single-electron processes. Additionally, this mechanism is considered to only play a minor role for the intersubband transitions of resonant phonon terahertz QCLs.[6,24] The dephasing rates $\gamma_{ij} = (\gamma_i + \gamma_j)/2$ are self-consistently determined from the outscattering rates

$$\gamma_i = \gamma_{\lambda\mathbf{k}} = \sum_{\lambda' \neq \lambda, \mathbf{k}'}{}' r'_{\lambda\mathbf{k}\to\lambda'\mathbf{k}'}, \tag{6}$$

where the prime above the summation sign indicates a summation over the various scattering mechanisms. In our simulation, the transition rates $r'_{i\to j} = r'_{\lambda\mathbf{k}\to\lambda'\mathbf{k}'}$ are obtained based on Eqs. (4) and (5), thus themselves depending on γ_{ij}. For this reason, several iterations of the EMC simulation have to be performed, until the obtained scattering and dephasing rates do not show significant changes any more. However, this does not necessarily constitute an additional numerical burden since iterative simulations are also required for the self-consistent calculation of the cavity light field,[25] and to properly take into account space charge effects.[24] Since the initially unknown dephasing rates γ_{ij} are calculated by counting the outscattering events over a whole iteration of EMC to obtain reliable statistics,[13] the first run has to be performed using conventional EMC. Subsequent iterations then employ the EMC method with CB corrections included (CB-EMC). Convergence is typically obtained after one EMC and two or three CB-EMC runs. Our treatment of CB is also compatible with other simulation approaches, such as hybrid density matrix-EMC.[20]

We test the influence of the implemented CB correction for two recently fabricated high temperature operation terahertz QCLs. In Fig. 1, the simulated current-voltage characteristics of (a) a record temperature 3.22 THz design[2] operating up to ~200 K and (b) a high temperature 1.8 THz design[3] operating up to 163 K is compared to the experiment. Results in Fig. 1 have been calculated at 10 K, and compared to the sampled experimental data of Refs. 2 and 3. The bias range of 7.6–10.8 kV/cm in Fig. 1(a) and of 5.5–10 kV/cm in Fig. 1(b) has been avoided in our calculations due to narrow anticrossings, which are known to produce unreliable results in EMC simulations.[20] First, we consider the LBR. Here, the classical implementation of EMC based on Fermi's golden rule clearly underestimates the current (squares), while the CB-EMC simulation shows good agreement with the experiment (circles). The reason is that for both structures, the electrons are at low biases injected into the lower laser level and have to make a transition to the upper laser level for being extracted to the phonon well. CB-EMC provides a ~10 times higher net scattering rate from lower to upper laser level than EMC for the 3.22 THz structure at 7.6 kV/cm, and a factor of ~9 increase is found for the 1.8 THz structure at 5.5 kV/cm. This results in

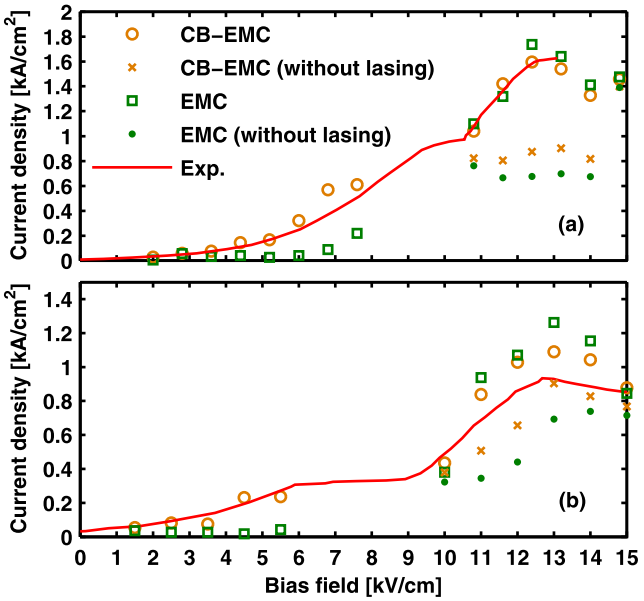

FIG. 1. Self-consistently calculated current density-bias characteristics and experimental results (corrected for bias drop) for a QCL from (a) Ref. 2 and (b) Ref. 3.

higher CB-EMC currents, suitably describing the experimental data.

The CB-EMC currents in the LBR are useful for estimating the voltage drop across the contacts in comparison to the experimental current-voltage curves, since, here, the waveguide loss is not required as an experimental input parameter. The best fit between the theory and experiment is obtained for a bias drop of 3.8 kV/cm (3.22 THz design) and 6 kV/cm (1.8 THz structure). The 3.8 kV/cm bias drop agrees well with the published results[2] if we consider a 10 μm active region, a 0.8 V drop across the top contact, and an additional $\sim$3 V drop resulting from contact removal.[2] The 6 kV/cm bias drop also qualitatively agrees with the 3–4 V reported in Ref. 3.

In the lasing regime, the simulation results including the influence of photon-scattering on the carrier transport[25–27] have been obtained assuming a total (waveguide and mirror) loss of 40 cm^{-1}, which is an upper estimate for the resonator loss in such structures.[2,28] Also, the current densities obtained without including the lasing field are displayed, corresponding to the parasitic current contributions due to non-radiative channels. While both the CB-EMC (circles) and EMC (squares) results with lasing included show reasonable agreement with the experiment, the currents obtained with conventional EMC somewhat exceed the CB-EMC results. Given that assuming a lower resonator loss[29] would result in stronger lasing activity and thus further increased currents in our simulation, the CB-EMC results tend to show a better agreement with the experiment than conventional EMC simulations. Interestingly, the parasitic current density obtained without including the lasing field is higher by up to $\sim$33% for CB-EMC (crosses) than for conventional EMC (dots). This indicates that the photon-induced current contribution is considerably reduced for CB-EMC as compared to conventional EMC, implying that the inclusion of CB leads to reduced gain and optical power.

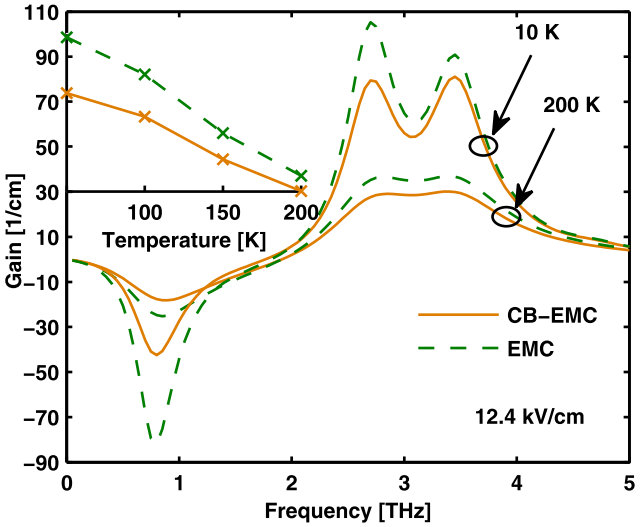

FIG. 2. Unsaturated spectral gain profile as obtained by conventional EMC and CB-EMC at a bias of 12.4 kV/cm, where the simulated current reaches its maximum. The inset shows the temperature dependent peak gain.

Fig. 2 shows the unsaturated spectral gain profile for the 3.22 THz QCL,[2] as obtained by CB-EMC (solid line) and EMC (dashed line). In the inset, the temperature dependent peak gain is shown. A significant peak gain reduction by about 20% from 105.4 cm^{-1} to 81.5 cm^{-1} at 10 K and from 36.9 cm^{-1} to 30.1 cm^{-1} at 200 K is observed when CB is included. This is largely due to a reduced population inversion, caused by less electrons in the upper laser level as well as more electrons in the lower laser level. Furthermore, we observe moderate broadening of the spectral gain profile from 1.27 THz (EMC) to 1.36 THz (CB-EMC) at 10 K and from 1.62 THz (EMC) to 1.64 THz (CB-EMC) at 200 K. The influence of CB on the spectral gain profile has also been investigated for other QCL structures. For a so-called phonon-scattering assisted injection and extraction design[30] at low temperatures (10 K), CB reduces the peak gain by only $\sim$7% at the peak current, while for the 1.8 THz structure[3] at 13 kV/cm the gain changes by 37% from 88.8 cm^{-1} (EMC) to 55.6 cm^{-1}(CB-EMC).

In Fig. 3, the influence of CB on the calculated output power is shown. For the 3.22 THz structure,[2] a reduction in the peak output power from 336 mW (EMC) to 245 mW

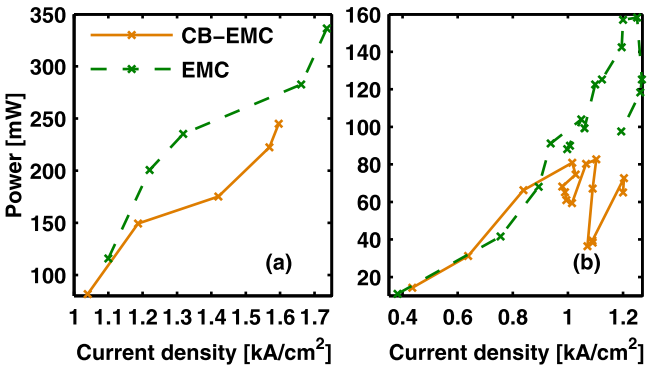

FIG. 3. Simulated power-current density characteristics at a lattice temperature of 10 K for (a) the 3.22 THz and (b) the 1.8 THz QCL. For (b), the CB-EMC output power at high current densities can decrease, similar to what was measured in Ref. 3.

(CB-EMC) is found (see Fig. 3(a)). A direct comparison to the experimental optical powers is not possible due to the unknown collection efficiency of the measurement setup. However, the maximum achievable current of 1.6 kA/cm^2 for CB-EMC is in line with the experiment.[2] In contrast, the conventional EMC simulation overestimates the maximum current density due to the higher predicted output power which results in an increased photon-induced current. This suggests that the CB-EMC output powers are more realistic. For the 1.8 THz structure[3] (Fig. 3(b)), a decrease in peak output power from 158.3 mW (EMC) to 80.9 mW (CB-EMC) is found, which is almost a factor of two. Again the range of obtained current densities agrees better with the experiment for the case of CB-EMC. Furthermore, the CB-EMC power-current curve at around 1 kA/cm^2 resembles the negative differential resistance feature observed in the experiment,[3] while this feature is missing in the EMC result.

In conclusion, collisional broadening has been self-consistently included into ensemble Monte Carlo carrier transport simulations, and its effect has been studied for several terahertz QCL designs. We find that the collisional broadening is crucial for the correct modeling of the current in the low-bias range. In the lasing regime, this effect leads to increased parasitic current as well as reduced optical gain and output power, resulting in a decreased photon-induced current contribution. Hence, better agreement with the experimental results in both the low-bias and the lasing regime is obtained.

A.M. and C.J. acknowledge support from the Emmy Noether program (DFG, JI115/1-1). C.J. also acknowledges funding by the Nanosystems Initiative Munich.

[1]M. Tonouchi, Nat. Photonics **1**, 97 (2007).
[2]S. Fathololoumi, E. Dupont, C. W. I. Chan, Z. R. Wasilewski, S. R. Laframboise, D. Ban, A. Mátyás, C. Jirauschek, Q. Hu, and H. C. Liu, Opt. Express **20**, 3866 (2012).
[3]S. Kumar, C. W. I. Chan, Q. Hu, and J. L. Reno, Nat. Phys. **7**, 166 (2011).
[4]F. Banit, S. Lee, A. Knorr, and A. Wacker, Appl. Phys. Lett. **86**, 41108 (2005).
[5]S.-C. Lee, F. Banit, M. Woerner, and A. Wacker, Phys. Rev. B **73**, 245320 (2006).
[6]T. Kubis, C. Yeh, P. Vogl, A. Benz, G. Fasching, and C. Deutsch, Phys. Rev. B **79**, 195323 (2009).
[7]C. Weber, A. Wacker, and A. Knorr, Phys. Rev. B **79**, 165322 (2009).
[8]R. Terazzi and J. Faist, New J. Phys. **12**, 033045 (2010).
[9]R. Köhler, R. C. Iotti, A. Tredicucci, and F. Rossi, Appl. Phys. Lett. **79**, 3920 (2001).
[10]H. Callebaut, S. Kumar, B. S. Williams, Q. Hu, and J. L. Reno, Appl. Phys. Lett. **83**, 207 (2003).
[11]O. Bonno, J.-L. Thobel, and F. Dessenne, J. Appl. Phys. **97**, 043702 (2005).
[12]J. T. Lü and J. C. Cao, Appl. Phys. Lett. **89**, 211115 (2006).
[13]C. Jirauschek and P. Lugli, J. Appl. Phys. **105**, 123102 (2009).
[14]L. Schrottke, M. Giehler, M. Wienold, R. Hey, and H. T. Grahn, Semicond. Sci. Technol. **25**, 045025 (2010).
[15]D. Indjin, P. Harrison, R. W. Kelsall, and Z. Ikonić, Appl. Phys. Lett. **82**, 1347 (2003).
[16]R. C. Iotti and F. Rossi, Appl. Phys. Lett. **76**, 2265 (2000).
[17]A. Mátyás, T. Kubis, P. Lugli, and C. Jirauschek, Physica E **42**, 2628 (2010).
[18]L. Reggiani, P. Lugli, and A.-P. Jauho, J. Appl. Phys. **64**, 3072 (1988).
[19]Z. Aksamija and U. Ravaioli, J. Appl. Phys. **105**, 083722 (2009).
[20]H. Callebaut and Q. Hu, J. Appl. Phys. **98**, 104505 (2005).
[21]R. C. Iotti, E. Ciancio, and F. Rossi, Phys. Rev. B **72**, 125347 (2005).
[22]I. Waldmüller, J. Förstner, S. Lee, A. Knorr, M. Woerner, K. Reimann, R. Kaindl, T. Elsaesser, R. Hey, and K. Ploog, Phys. Rev. B **69**, 205307 (2004).
[23]R. W. Boyd, *Nonlinear Optics* (Academic, New York, 2003).
[24]C. Jirauschek, A. Mátyás, and P. Lugli, J. Appl. Phys. **107**, 013104 (2010).
[25]C. Jirauschek, Appl. Phys. Lett. **96**, 011103 (2010).
[26]I. Bhattacharya, C. W. I. Chan, and Q. Hu, Appl. Phys. Lett. **100**, 011108 (2012).
[27]A. Mátyás, P. Lugli, and C. Jirauschek, J. Appl. Phys. **110**, 013108 (2011).
[28]A. Matyas, R. Chashmahcharagh, I. Kovacs, P. Lugli, K. Vijayraghavan, M. A. Belkin, and C. Jirauschek, J. Appl. Phys. **111**, 103106 (2012).
[29]D. Burghoff, C. W. I. Chan, Q. Hu, and J. L. Reno, Appl. Phys. Lett. **100**, 261111 (2012).
[30]E. Dupont, S. Fathololoumi, Z. R. Wasilewski, G. Aers, S. R. Laframboise, M. Lindskog, S. G. Razavipour, A. Wacker, D. Ban, and H. C. Liu, J. Appl. Phys. **111**, 073111 (2012).